WATER RESOURCES RESEARCH, VOL. 37, NO. 4, PAGES 857–871, APRIL 2001

Overpressures in the Uinta basin, Utah: Analysis using a three-dimensional basin evolution model

Brian J. O. L. McPherson
Hydrology Program, New Mexico Institute of Mining and Technology, Socorro

John D. Bredehoeft
The Hydrodynamics Group, Edmonds, Washington

Abstract. High pore fluid pressures, approaching lithostatic, are observed in the deepest sections of the Uinta basin, Utah. Geologic observations and previous modeling studies suggest that the most likely cause of observed overpressures is hydrocarbon generation. We studied Uinta overpressures by developing and applying a three-dimensional, numerical model of the evolution of the basin. The model was developed from a public domain computer code, with addition of a new mesh generator that builds the basin through time, coupling the structural, thermal, and hydrodynamic evolution. Also included in the model are in situ hydrocarbon generation and multiphase migration. The modeling study affirmed oil generation as an overpressure mechanism, but also elucidated the relative roles of multiphase fluid interaction, oil density and viscosity, and sedimentary compaction. An important result is that overpressures by oil generation create conditions for rock fracturing, and associated fracture permeability may regulate or control the propensity to maintain overpressures.

1. Introduction

The condition whereby pore fluid pressure greatly exceeds hydrostatic pressure is known as overpressure and is prevalent in the deeper, low-permeability sections of sedimentary basins throughout the world. Economic interest in sedimentary basin overpressures exists because zones of overpressure may indicate the presence of oil or gas [*Timko and Fertl*, 1971; *Spencer*, 1987]. Another motivation for this study is that overpressures are often cited as a driving force for groundwater flow and are associated with many other hydrogeologic processes [*Garven*, 1995; *Neuzil*, 1995].

Overpressures develop when fluids completely fill available pore space and fluid expulsion is not rapid enough to maintain normal or equilibrium pressure conditions. This situation may occur when pore space is compacted by sedimentary deposition [*Bethke*, 1986] or tectonic compression [*McPherson and Garven*, 1999]. Alternatively, pore fluid volume may increase if new fluid is generated in situ by geochemical processes such as hydrocarbon generation.

The case study area considered is the Uinta basin, Utah, a textbook example of an overpressured sedimentary basin [*Domenico and Schwartz*, 1990]. Overpressures observed in the northern half of the Uinta basin approach lithostatic pressure [*Fouch et al.*, 1992], and are thought to result from hydrocarbon generation, based on geologic inference and modeling studies [*Spencer*, 1987; *Sweeney et al.*, 1987; *Bredehoeft et al.*, 1994]. *Bredehoeft et al.* [1994] based such a conclusion on a three-dimensional (3-D) numerical model of the hydrodynamics of the present-day basin. The *Bredehoeft et al.* [1994] study considered only single phase (water) flow, and its conclusions were therefore limited. This study is intended to revisit the problem, but to evaluate the problem in much more detail including (1) explicit treatment of the geologic history, including sedimentation and compaction, uplift, subsidence and erosion, and changes in rock properties associated with these processes, (2) the 3-D thermal and hydrodynamic history produced by such a model, and (3) in situ generation of hydrocarbons with multiphase flow of oil and water with appropriate relative permeability and capillarity effects. We evaluated the relative effects of these processes and associated parameters in creating and maintaining overpressures. In particular, we simulated end-member possibilities of the geologic history, and conducted a sensitivity analysis to elucidate the roles of other processes.

Paper number 2000WR900260.
0043-1397/01/2000WR900260$09.00

2. Geologic Setting and History

The Uinta basin of northern Utah (Figure 1) lies along the northern edge of the Colorado Plateau. The basin developed during the Laramide orogeny of latest Cretaceous and early Tertiary age (75 to 50 Ma). It is structurally asymmetrical to the north (Figure 2a) and is elliptical with its major axis almost due east-west. The deepest sections are in the northern third of the basin, in the area of the Altamont oil field (Figure 1). This area is bounded by a large basement thrust fault that dips northward [*Fouch et al.*, 1992]. Higher topography surrounds the basin (Figure 1). These adjacent highlands are sources of Tertiary sediments [*Hintze*, 1980], which approach 6 km thickness in the northern part of the basin.

This study focuses primarily on the Tertiary Green River Formation. Figure 2b shows a generalized stratigraphic column of the Green River Formation, which is an Eocene lake deposit consisting of intercalated sandstones, shales, mudstones, and carbonates, especially dolomite. The Green River Formation is also common to many other Laramide basins in the region, including the Bridger basin, Washakie basin, and the Piceance Creek basin. Within the Uinta basin the Green River Forma-

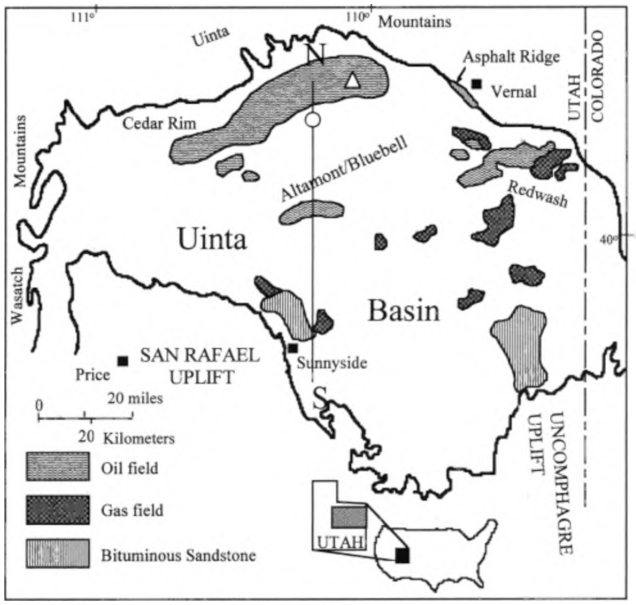

Figure 1. Location map of the Uinta basin, Utah. Location of profile N-S is indicated on the map, as are most oil and gas production fields.

tion consists of three primary depositional facies [*Ryder et al.*, 1976]: open lacustrine, marginal lacustrine, and alluvial. In this system the open lacustrine facies consists primarily of mud-supported carbonates and other organic-rich sediments, the marginal lacustrine facies consists primarily of claystones, sandstones, and carbonates associated with lake-margin deltaic and interdeltaic environments, and the alluvial facies consists primarily of channel sandstones to very fine grained sandstones and claystones. Strata in both open lacustrine and marginal lacustrine facies are source rocks for oil and gas in the basin, especially oil shale. Above the Green River Formation are the Uinta and Duchesne River Formations (Figures 1 and 2), mixed fluvial and lacustrine units deposited during the final stages of subsidence [*Johnson and Nuccio*, 1993].

Fouch et al. [1992] provides updated maps of facies for several isochronous horizons in the Uinta basin. The cross section in Figure 2a shows only general stratigraphic boundaries. The basin's actual stratigraphy is fairly complex, however. Our models of the basin include the complex stratigraphy described by *Fouch et al.* [1992], inasmuch as we digitized their facies mappings [*McPherson*, 1996].

Laramide tectonism dominated the region of the Uinta basin from Late Cretaceous up to the Oligocene. Uplifts of the Uinta and Wasatch mountains (Figure 1) initiated by latest Cretaceous. Associated subsidence created shallow basins and lakes, with deposition occurring in alluvial/fluvial, wetland, and shallow lacustrine environments. The San Rafael swell south of the Uinta basin is also a Laramide structure. It is a large northeast trending anticline with gently dipping fans, but it is not and probably never was a major topographic high [*Johnson and Nuccio*, 1993]. This anticline and the Uncomphagre uplift are partially responsible for the gentle northern dip of the southern half of the basin. Uplift began during the late Cam-

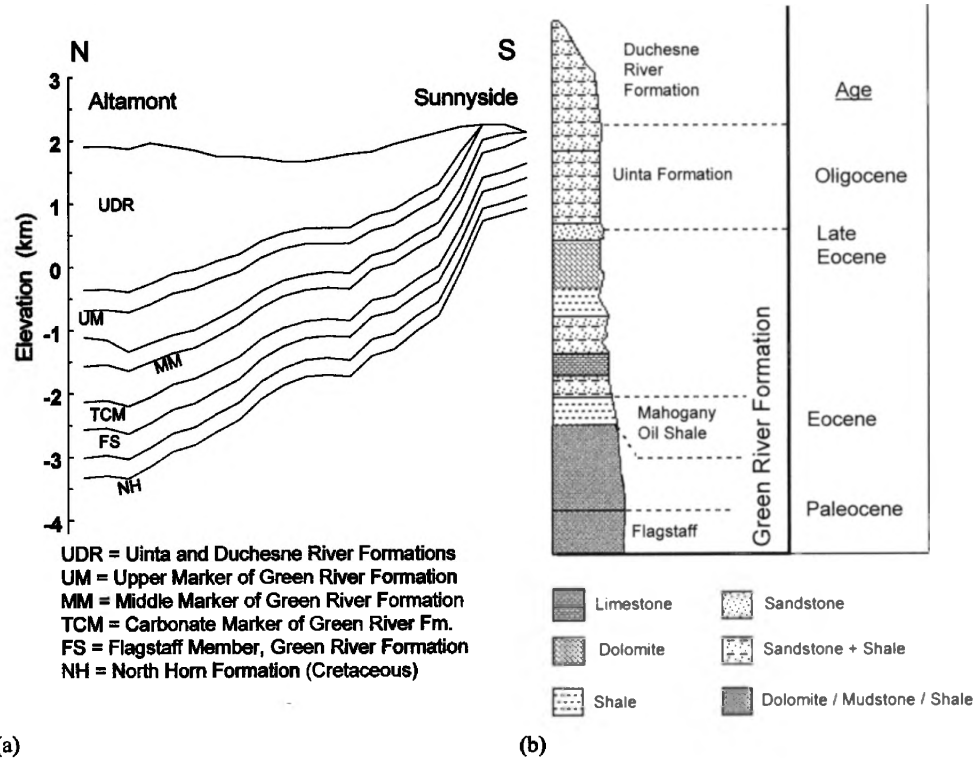

Figure 2. Generalized stratigraphy and structure of the Uinta basin. (a) Structural cross section N-S (location of profile N-S shown on Figure 1), vertical exaggeration equal to 20. (b) Generalized stratigraphic column of the Tertiary formations. The lines on the cross section demarcate the hydrostratigraphic units used in the basin evolution model. See *Ryder et al.* [1976] and *Fouch et al.* [1992] for an explanation of stratigraphic terms and for detailed stratigraphic variations that are mapped into the numerical model but not shown on this cross section.

panian [*Franczyk et al.*, 1990] and continued until late Eocene. Between the San Rafael swell, the Uncomphagre uplift, and the contemporaneous subsidence adjacent to the Uinta and Wasatch uplifts, the basin's ultimate bowl-like shape probably began to take form around this time.

In summary, the bowl-shaped Uinta basin formed during the Laramide orogeny, with timing of uplifts, subsidence, and deposition beginning in the early phases of orogenesis, and ending probably during the Oligocene or later. The geologic history and its effects on the fluid migration and thermal histories of the basin are discussed and explored in more detail by *McPherson* [1996].

3. Observed Fluid Pressures

Among the most interesting aspects of the Uinta basin are the significant overpressures observed in northern areas. Mapped in Figure 3 is an isometric projection of observed hydraulic head at the stratigraphic equivalent to the Flagstaff member of the Green River Formation (Figure 2), illustrating the extremely high heads in the Altamont area compared to the surrounding ambient head distribution. Figure 4 is a pressure-depth profile in the Altamont oil field. Original data used to create this profile are published by *Bredehoeft et al.* [1994]. Maximum observed pressures in this particular area of the field are 65 MPa, or 27.5 MPa overpressure, where "overpressure" is explicitly defined as the amount of pressure above hydrostatic fluid pressure. While this pressure is measured at ~4 km depth (~ −1.5 km below sea level), it is equivalent to ~5.1 km hydraulic head. The maximum observed fluid pressure in the Altamont area, as well as the entire basin, is equivalent to 6065 m head, about 3 km higher than the maximum topography, at ~4 km depth. Highest anomalous pressures are observed within the deepest sections of the Green River Formation and are thought to be associated with oil generation [*Spencer*, 1987]. Fluid pressures decrease to normal in the North Horn Formation, below the oil production interval of the Green River Formation. Substantial overpressuring, caused by generation of natural gas, is speculated to be present in the Cretaceous Mesaverde Group below the Altamont field [*Spencer*, 1987; *Fouch et al.*, 1992].

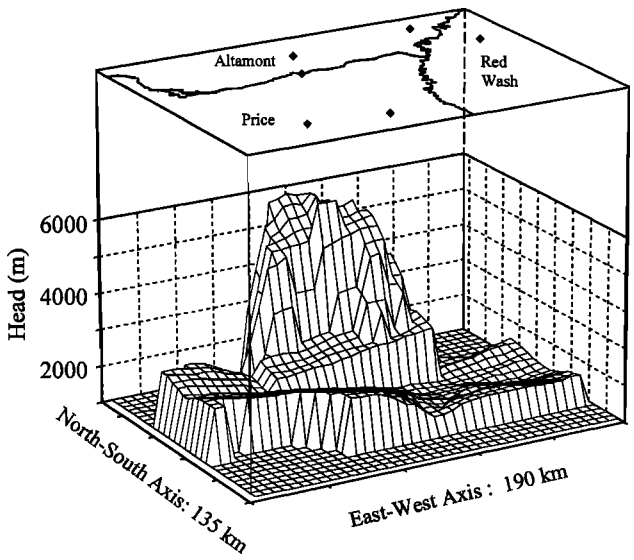

Figure 3. Isometric projection of observed hydraulic head in the Flagstaff member of the Green River Formation within the Uinta basin.

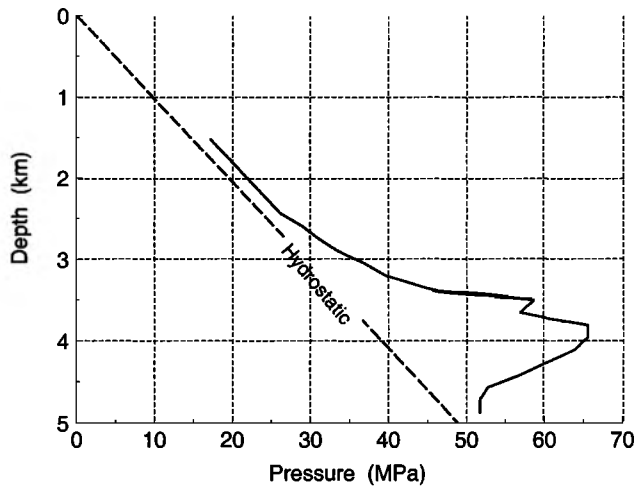

Figure 4. Observed fluid pressure-depth profile in Altamont field (adapted from *Bredehoeft et al.* [1994]. Shown for reference is a hydrostatic pressure profile (freshwater; dashed line).

In the highly overpressured area of the Uinta basin (Figure 3), oil source rocks are abundant, and more oil is produced than anywhere in the state of Utah. The oil production map for the state (Figure 1) shows geographic coincidence between the Altamont oil field and the primary area of observed overpressures (Figure 3). These facts suggest that oil generation is the primary overpressure mechanism.

Other common overpressure mechanisms include depositional pore compaction, clay dewatering by diagenesis, aquathermal pressuring, and tectonic compression. However, with the exception of depositional compaction, each of these is easily ruled out as a possible mechanism. Our analysis indicates that depositional compaction can also be ruled out, as it can cause a nearly insignificant amount of overpressuring.

4. Numerical Model of Basin Evolution

Rather than spending great effort building a three-dimensional numerical model from scratch, an initial goal of this study was to use a public domain simulation code. We selected TOUGH2 [*Pruess*, 1991], a public domain geothermal reservoir simulator developed at the Lawrence Berkeley Laboratory, for our purposes. TOUGH2 was specifically designed to simulate coupled heat and multiphase fluid transport in porous and fractured media. We examined and tested several simulators before using TOUGH2, and concluded that TOUGH2 offered the following advantages for this study: (1) it is a three-dimensional simulator, (2) it is well known, currently used by many workers, and has been tested against several other geothermal reservoir simulators [*Pruess and Wang*, 1984; *Moridis and Pruess*, 1992; *Oldenburg and Pruess*, 1994], and (3) it uses an integrated finite difference method [*Narasimhan and Witherspoon*, 1976], the advantages of which we discuss below.

The primary code development effort on our part was to develop a new set of routines, which we call "Dynamic Mesh Evolver" (DYME), that generates the integrated finite difference mesh, and evolves its parameterization and boundary conditions according to the geologic history imposed. DYME

Table 1. Summary of General Mass and Energy Conservation Equations Solved by TOUGH2[a]

	Equation	Parameter
General mass conservation equation	$\frac{\partial}{\partial t}\int_V\int\int M\,dV = \int_S\int \mathbf{F}\cdot\hat{n}\,dS$	$\mathbf{F}$, mass flux vector M, mass V, volume
Conservation equation expressed at and between elements n and m (M is total connected elements to element n)	$V_n M_n = \sum_M A_{nm}F_{nm}$	A, area
Darcy's law for fluid flow	$\mathbf{F}_{\text{fluid}} = -k\sum_\beta \frac{k_\beta}{\mu_\beta}\rho_\beta(\nabla p - \rho_\beta \mathbf{g})$	k, permeability k_β, relative permeability with respect to phase β μ_β, viscosity of phase β ρ_β, density of phase β $\mathbf{g}$, gravitation acceleration ∇p, pressure gradient
Fourier's law for heat flow plus advective heat transfer	$\mathbf{F}_{\text{heat}} = -\lambda\nabla T + \sum_\beta h_\beta \mathbf{F}_\beta$	H_β, specific enthalpy of phase β $\mathbf{F}_\beta$, mass flux of phase β λ, thermal conductivity ∇T, temperature gradient

All equations apply to both water and oil fluid phases (phase-specific terms indicated by subscript; β is oil, or β is water). Information is summarized from *Pruess* [1987].

and TOUGH2 simulate the basin's evolution together, in a fully coupled fashion; a layer of finite difference cells is added to simulate addition of a new formation, and those cells are thickened to simulate sedimentation. Sediments are always initially deposited horizontally. Similarly, a layer of cells is thinned to simulate erosion, and that layer of cells is removed when the entire formation is eroded. Cells are moved with respect to each other to simulate differential uplift or subsidence. With this dynamic mesh the transient effects of sedimentation, erosion, and structural changes (uplift and subsidence) on the hydrogeological and thermal aspects of the basin are explicitly considered. We also needed to add compaction source/sink terms to the governing equations of TOUGH2, described in Appendix A of this paper.

At the start of a simulation the basal layers of the mesh are generated by DYME. During each time step the mesh is modified by DYME according to the basin's history (e.g., subsidence, deposition, uplift, erosion, etc.), and this mesh and its properties are passed to TOUGH2 for assembly and solution of the equations of mass and energy transport. The general forms of these equations, tabulated in Table 1, account for flow of water, flow of oil, and flow of heat, including conductive and advective components. Variations in fluid flow, heat flow, and material properties may be examined for any slice of the 3-D mesh at any time during the basin's history.

The integrated finite difference method is particularly appropriate for modeling with a dynamic mesh. The finite element method requires that each element be constructed so that its aspect ratio (the ratio of maximum to minimum element dimensions) is close to unity, at least for isotropic materials. Aspect ratios can be higher than 1, but a value exceeding 5 should be avoided; otherwise, numerical instabilities or errors may result. The finite difference method is not as prone to aspect ratio problems, but finite difference grids must be rectangular. The integrated finite difference method offers the mesh flexibility of the finite element method without the aspect ratio constraints, making the method particularly useful for modeling active sedimentation. A layer begins as a thin veneer of sediment, and thus cells representing it can have very large aspect ratios at the initial stage of deposition. Additionally, the integrated finite difference method offers the numerical robustness (at high nodal aspect ratios) of the finite difference method without the regular, rectangular grid spacing constraints. This property is beneficial for simulation of later stages of the basin's history when differential uplift and flexure induce variable curvature in the basin structure. Additionally, the public domain TOUGH2 package includes a suite of conjugate gradient solvers [*Moridis*, 1995] that are particularly robust in light of the extreme, nonlinear changes in porosity and permeability (in space and time) that occur during a typical basin evolution simulation.

4.1. Summary of the Algorithm

1. Initial layers of mesh are generated by DYME. For the Uinta basin simulations this includes Cretaceous and older units considered.
2. At each time step the equations of fluid flow (including groundwater and oil) and heat flow are assembled and solved. Appropriate equations of state are used to evaluate density, viscosity, and enthalpy of groundwater and oil.
3. During a time step in which sedimentation of a new formation begins, a new layer(s) of finite difference cells is added to the model domain mesh. Each new layer is assigned an initial thickness of 1 m (to minimize numerical instability associated with extreme aspect ratios), and thickening of the layer begins at the time when deposition would have accumulated 1 m of sediment. Cells thicken at a rate equal to the sedimentation rate.
4. Changes in effective stress and resulting compaction (collapse of pore space) are calculated and applied for each cell (see Appendix A).
5. Changes in permeability as dictated by porosity changes (solid line on Figure 5) are applied for each cell.
6. Structural changes, including thickening of layers due to sedimentation, thinning, or removal of layers by erosion, and

layer curvature caused by differential uplift/subsidence are applied.

7. The time-temperature history up through the current successful time step is integrated, and resulting oil generation rate and cumulative amount of oil generated for each oil source cell are computed based on the prescribed total organic carbon (TOC). Initial TOC is based on facies designation, and the amount present is reduced by the amount converted to oil. Porosity equivalent to this amount is also created.

8. The amount of oil generated from kerogen, determined for the previous time step, is injected at the source cells to simulate oil expulsion.

9. The amount of water that compaction expels from pore space within each individual cell, determined from the previous time step, is injected to account for changes in fluid mass balance associated with compaction (see Appendix A). Fracture permeability is also induced at this point, as described in a subsequent section below.

Steps 2 through 9 are repeated at each time step. Described below are details of how the DYME algorithm is used to assemble and simulate the basin's history. For a description of the TOUGH2 algorithm, including more details of the governing equations and solution method, see *Pruess* [1987] and [1991].

4.2. Model Grid

The numerical model mesh used to simulate the Uinta basin was relatively coarse. Most of the 14 layers in the grid consisted of cells with horizontal length dimensions of around 5 km, and ranging in thickness from tens of meters to ~500 m. Computational capacity limited the grid spacing and resolution, but simulations we conducted using finer gridding (but smaller areas of the basin) suggest that the resolution is acceptable for studying regional overpressures. Selected areas of the Green River Formation, including the Flagstaff and adjacent overpressured layers, were somewhat more finely gridded, with cells of the order of 1 km in width and 100 m in thickness. The final 3-D model grid assembled in each history simulation consisted of just over 11,000 cells. Every evolution simulation begins with one layer of active cells, with more layers added during the course of the basin's history, finishing with 11 active layers. Another 4 layers of cells are located below the basin model domain for the purpose of extending basal heat flow sources to 50 km below the basin. Such distance is necessary to properly simulate the transient thermal response of basin strata to changes in surface temperature and other conditions. Otherwise, if basal heat flow sources are located too close to the active basin domain, strata at the base of the basin track the temperature of the heat sources.

4.3. Assembling and Simulating the Basin History

Developing and simulating the basin history requires a great amount of geologic information and several detailed steps, as follows.

4.3.1. Basin structure and stratigraphy. Assemble the present three-dimensional structure and stratigraphy of the basin, and construct a template of the numerical mesh that DYME will build and evolve. Figure 2a, structural cross section N-S, shows the breakdown of eight individual stratigraphic layers serving as discrete model layers for our analysis, drawn from structure contour maps of *Bredehoeft et al.* [1994].

4.3.2. Backstripping and stratigraphic projection. Estimate sedimentation rates for each layer at all points in the basin. We used a backstripping method [*Allen and Allen*, 1992] for estimating sedimentation rates at each column of the model grid. Modeled formation contact elevations were within 1% of observed contact locations. Additionally, layers that crop out at the surface were stratigraphically projected [*McPherson*, 1996] to provide an estimate of material deposited but since eroded.

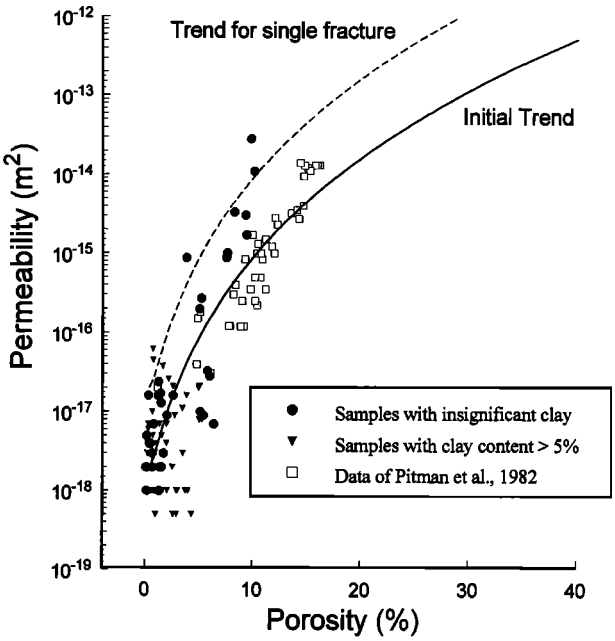

Figure 5. Permeability of Uinta basin samples, plotted against porosity. Solid circles represent permeabilities from unfractured samples with no clay present. The solid triangles represent permeability from unfractured samples with clay present, illustrating how any clay can significantly reduce permeability. The open squares are data from *Pitman et al.* [1982]. The solid line is a least squares regression fit (with exponential form equation) through the no-clay data and the data of *Pitman et al.* [1982]. The dashed line is the permeability/porosity relationship tracked by a fractured cell (discussed in the text).

4.3.3. Estimate amount and timing of uplift and erosion. The amount of uplift or subsidence at each column in the basin model grid is simply the difference in elevation between the beds at their estimated maximum depth and their present structural elevation. Uplift/subsidence rates are assumed to be constant through time and equal to the magnitude divided by the duration of uplift/subsidence. As model strata cross the specified present-day surface, they are stripped off or eroded. Erosion in the model is simulated by reducing the thickness of a cell as it intersects the specified erosional surface. The reader is referred to *McPherson* [1996] and *McPherson and Garven* [1999] for more details regarding this and steps 1–2 above.

4.4. Boundary Conditions

The following boundary conditions were applied during the model simulations:

1. A uniform, constant basal heat flow was applied at the basal boundary (50 km depth, as described previously). We assigned the basal heat flow to be 65 mW m^{-2}, the value necessary to fix the present-day average surface heat flow in the northern third of the basin at 57 mW m^{-2}, the average surface heat flow value for that region estimated by *Chapman*

et al. [1984]. *McPherson* [1996] details the effects of variations in this boundary condition.

2. A specified surface temperature history (temperature versus time) was used to govern the surface boundary temperature. In some simulations the surface temperature was held constant, and in others it varied through time, as discussed in subsequent sections.

3. Constant head, equal to surface topography minus 100 m, was assigned at the surface of the domain throughout the history simulation. Values of hydraulic head in most intracontinental groundwater systems are within 100 m of the surface and are stable with time [*Hubbert and Rubey*, 1959].

4. No-flow boundaries were assigned at the sides and bottom of the model domain. We assumed that the permeability of shale layers below the Cretaceous North Horn Formation provides a low-permeability barrier that justifies a no-flow boundary. Because portions of the Cretaceous section crop out in most areas of the basin, no-flow boundaries were assigned to the entire base/sides of the model except at the Uinta mountain boundary, where the Uinta south flank fault is a prescribed no-flow interface. A specified flux boundary was assigned to the southern periphery of the model, justified by inferred fluid flow out of the basin through the Mesa Verde Group to the south (M. Person, written communication, 2000).

4.5. Fractures and Fracture Generation in the Model

General knowledge of the character and distribution of fractures is helpful for interpreting the hydrodynamic regime because of the effects of fractures on permeability. Throughout the Altamont/Bluebell fields are vertical to nearly vertical, mineralized, open fractures that enhance oil production [*Lucas and Drexler*, 1976]. Extensive subsurface systems of fractures are thought to exist, and significant regional systems of fractures and joints are evident at the surface. Fracture and joint systems of the Uinta basin in general are discussed and reviewed by *Chidsey and Laine* [1992] and *Narr and Currie* [1982].

The permeability data used in this study (Figure 5) were measured on core samples and are explicitly valid only for the core scale. Well-scale to regional-scale permeabilities, measured or inferred, can be very much higher than core-scale permeabilities measured for the same strata [*Deming*, 1993; *Willett and Chapman*, 1987; *Neuzil*, 1986]. In the Uinta basin specifically, *Bredehoeft et al.* [1994] published 78 well-scale permeabilities inferred from drill stem test analyses that cover much of the depth section, and at any given depth these data span 2 to 6 orders of magnitude. The variability is attributed to fractures that the core scale measurements do not sample. It is inappropriate to assume that the core-scale permeabilities sufficiently describe the well-scale and basin-scale permeabilities. We addressed this problem by inducing fractures during the model simulation; if fluid pressure in a cell exceeded the least principal stress, the permeability of that cell was increased by a specified amount in all directions. In other words, fracture permeability was simulated by increasing the matrix permeability. We assumed principal stress for the Uinta basin to be 0.80 times lithostatic pressure, the same value determined for the adjacent Piceance basin by *Bredehoeft et al.* [1976]. The magnitude of fracture permeability enhancement was arbitrary; a single order of magnitude increase of permeability was assigned for a single fracture; more than 1 order of magnitude permeability increase would occur if a single cell fractured more than once. In most model simulations, lateral fracture networks of several kilometers develop, and thus the regional-scale permeability is increased. No fracture annealing (for example, by calcite precipitation within fractures) is built into the model. However, permeability of fractured cells continues to change with porosity at the same rate as unfractured cells, but at an order of magnitude higher value (dashed line on Figure 5).

5. Data and Model Parameterization

For the sake of brevity, parameterization of the numerical model, including measured and assumed values of rock and fluid properties such as permeability, porosity, thermal conductivity, sedimentary facies, oil density, and oil viscosity are detailed by *McPherson* [1996] and *McPherson et al.* [2001]. Also discussed by *McPherson* [1996] are thermal aspects such as heat flow calibration and the kinetic model and data used for in situ oil generation in the model. *McPherson et al.* [2001] discusses in much more detail porosity, permeability, and lithology measured of Uinta basin rocks for this study.

6. Analysis and Results

6.1. End-Member Cases of Geologic History Investigated

Determining and simulating the exact geologic history of the Uinta basin was not among our objectives. Rather, we attempted to understand how different geologic conditions through time affect fluid pressures, thermal conditions, and fluid migration. In this study we evaluated two "end-member cases," or possibilities, of the geologic history. The two cases have identical depositional histories, but differ in terms of timing of the uplift and erosion that form the "bowl" shape of the basin.

The first of these we call the "late uplift model." In this conceptual model of the basin's history, all rock layers are deposited when their ages dictate, but all uplift and erosion of the basin's periphery (forming the basin's bowl shape) occur from 10 Ma to the present. Figure 6 displays this burial history for a single package of sediment at a point location along the southern periphery of the basin. This timing is coincident with regional uplift of the Colorado Plateau known to occur during the Miocene.

We call the second end-member case the "early uplift model." In this model all uplift and erosion of the basin's periphery are contemporaneous with deposition of Tertiary strata during the Laramide orogeny. As such, all "extra" rock material estimated by stratigraphic projection is eroded very early in the simulation. The dashed curve on Figure 6 represents this burial history for a single point at the southern periphery of the basin. For reference, the published burial history of *Anders et al.* [1992] associated with the same strata but in the deepest part of the basin near Altamont (Figure 1) is also drawn on Figure 6. The history of *Anders et al.* [1992] is calibrated via a modified Lopatin approach, but timing of uplift phases is not certain, nevertheless. Our end-member conceptual models draw on the *Anders et al.* [1992] study, the *Johnson and Nuccio* [1993] study, and others as described by *McPherson* [1996]. Our conceptual history is not calibrated for its depth history by geochemical or other means (for example, by vitrinite reflectance or isotopes), as such calibration is beyond the scope of this study and would warrant a completely separate project. The reader is referred to *Johnson and Nuccio* [1993] for details of such a study of the Uinta basin.

Our goal is to determine what is the likely range of possible

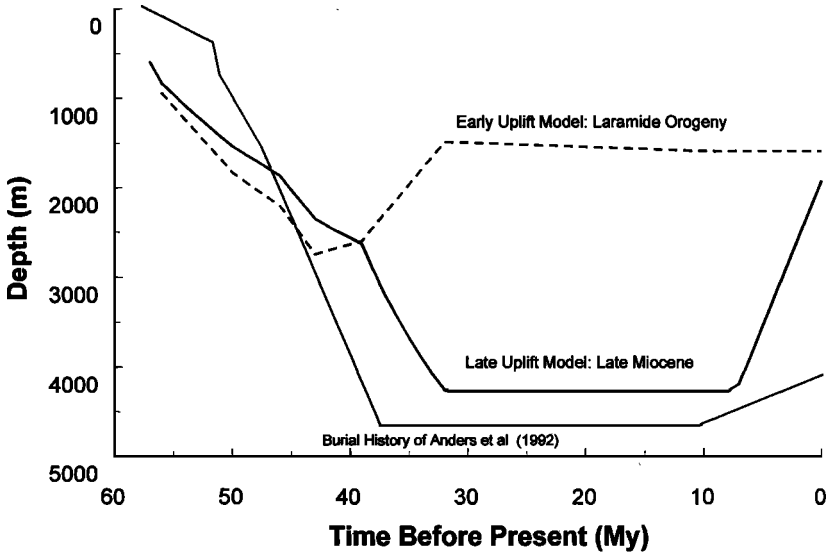

Figure 6. Burial histories corresponding to the early uplift model (dashed line) and the late uplift model (solid line) for strata close to Sunnyside on the southern periphery of the Uinta basin. Also illustrated is a burial history published by *Anders et al.* [1992] for a location in the Altamont field (Figure 1).

overpressure effects of the geologic or burial history of the basin. In the following sections, we discuss both conceptual model histories, including the ramifications and simulation results concerning overpressure development and maintenance. *McPherson* [1996] evaluates in more detail the effects of the different histories on the basin's thermal and fluid migration histories. Much of our discussion focuses on results for strata near the Altamont area because it is the site of highest observed overpressures.

6.2. Subsurface Temperature History Results

We paid particular attention to the subsurface temperature history because it is the most important factor in determining the timing, rates, and amounts of hydrocarbon generation. In turn, the timing and amounts of hydrocarbon generation influence overpressure development and the hydrodynamic history.

Except for basal heat flux into the basin from below, the structural/depth history is the primary control on the temperature history. Figure 7 portrays the late uplift model burial histories for strata at a single location (open triangle on Figure 1) along the northern edge of the Altamont oil field. Subsurface temperature histories associated with these burial histories are depicted in Figure 8. Temperature at each horizon increases as depth increases, tracking the ambient thermal gradient. When deposition ceases at 32 Ma, temperature continues to increase at a slower rate due to conductive equilibration of the sedimentary column. *Chapman and Furlong* [1992] discuss in detail this type of temperature equilibration following deposition. As uplift and erosion of the sedimentary section occur during the last 10 Myr of the history, temperature decreases as depth decreases.

Many factors influence the temperature history, including effects of thermal conductivity structure, erosion, sedimenta-

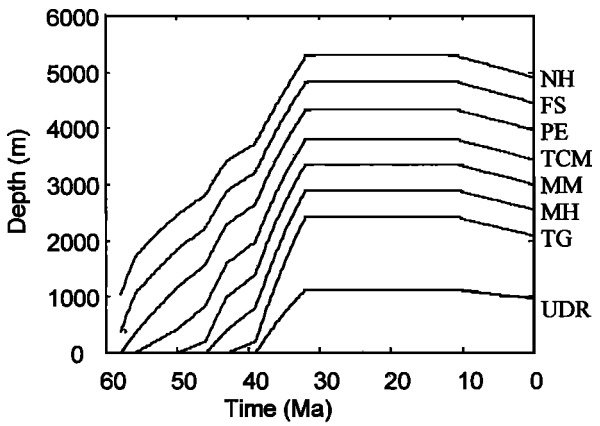

Figure 7. Burial history for strata at the northernmost edge of the Altamont oil field, late uplift model. Key: UDR, Uinta and Duchesne River Formations; TG, Top of Green River Formation; MH, Mahogany Oil Shale; MM, Middle Marker of Green River Formation; TCM, Top of Carbonate Marker within Green River Formation; PE, Paleocene-Eocene Boundary; FS, Flagstaff member of Green River Formation; NH, North Horn Formation (Cretaceous).

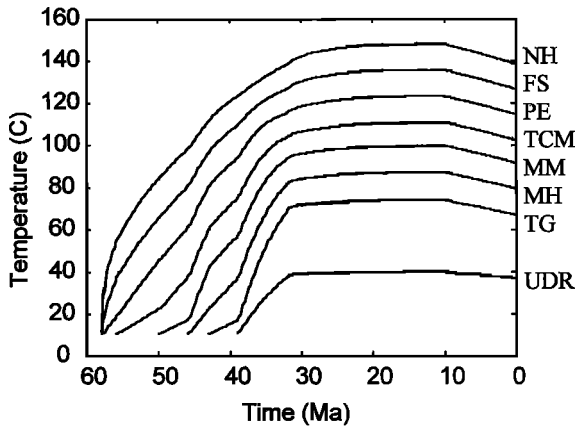

Figure 8. Temperature history for strata at the northernmost edge of the Altamont oil field, late uplift model. See caption of Figure 7 for key of abbreviations.

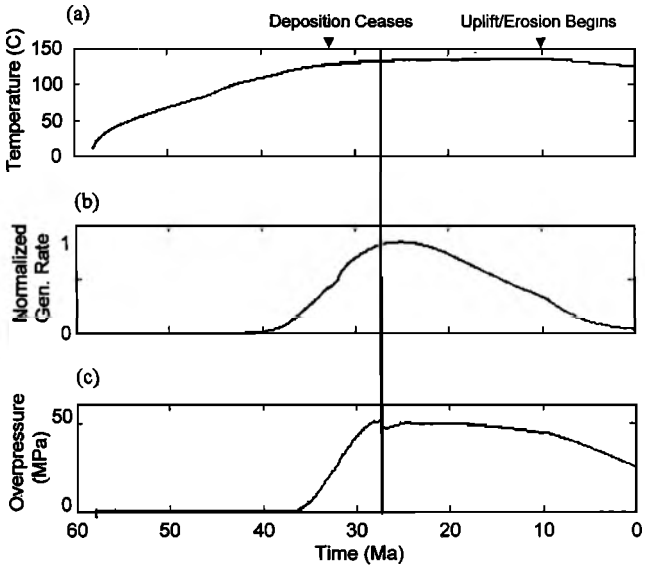

Figure 9. Correlation between temperature history and overpressures for the Flagstaff member of the Green River Formation at the northernmost edge of the Altamont field: (a) modeled temperature history, (b) oil generation rate history, and (c) overpressure history.

tion, and advection by groundwater. All of these effects are explicitly treated in the model. The thermal aspects applied in this model, including basal heat flow, thermal conductivity structure, and calibration of modeled heat flow budget to observed heat flow data, are described by *McPherson* [1996].

6.3. Process of Overpressuring by Oil Generation and the Role of Temperature

The correlation between temperature history and overpressures is illustrated by Figure 9, including the modeled temperature history (Figure 9a), oil generation rate history (Figure 9b), and overpressure history (Figure 9c) for the Flagstaff member of the Green River Formation at the northernmost edge of the Altamont field. These results correspond to the late uplift model with a constant surface temperature boundary condition ($T_{surface}$ = 11°C). During the depositional phase from 56 to 32 Ma, temperature in the Flagstaff increases as depth increases (Figure 9a). Temperature reaches the "oil window," or temperature range in which kerogen to oil conversion is significant, at about 40 Ma (Figure 9b). Overpressure (plotted in Figure 9c), or the amount of pressure above the hydrostatic condition, becomes significant at ~37 Ma, shortly after oil conversion rates become significant. The chemical reaction that converts kerogen to oil approaches its peak at 28 Ma, and the peak in overpressures is coincident (see vertical reference line on Figure 9). A sudden drop in pressure (crossed by vertical reference line in Figure 9c) occurs due to an induced fracture at ~27.5 Ma; when fluid pressure exceeds the value of least principal stress, a vertical fracture is simulated by increasing vertical permeability 1 order of magnitude (refer to Figure 5, the permeability data plot, and associated discussion). During the last 25 Myr of the basin's history the temperature of the Flagstaff remains in the "oil window," yet the oil generation rate decreases to close to zero by present day. The rate reduction is attributable to the chemical reaction reducing available kerogen for conversion. We were led to infer that overpressures are associated with oil generation because overpressure dissipation coincides with oil generation rate reduction, much as overpressure increase is coincident with increases in oil generation rates. A sensitivity analysis verified the conclusion. Overpressures dissipate slowly, but not completely, because permeability of the Flagstaff is fairly low. The rate of dissipation suggests that another 10 to 15 Myr will be required for overpressures to disappear completely.

6.4. Overpressure Development: Model Results and Determining Factors

When we simulated the basin's evolution with geologically reasonable parameters, the modeled fluid pressure regime was consistent with the observed overpressure distribution. Figure 10 is a map of hydraulic head results for the Flagstaff member, corresponding to the late uplift model at present day. Comparing this map to the map of observed hydraulic head (Figure 3) illustrates that the model qualitatively reproduces observed overpressures, including peak overpressure approaching 6 km head in the northernmost part of the basin. For a quantitative comparison, Figure 11 is a grey-scale contour mapping of the disparity between modeled overpressures (for this particular model) and observed. The vast majority of the Flagstaff reflects a small difference between modeled and observed pressures. However, large negative differences (observed much greater than modeled) are located in the northern part of Altamont (darkest contours on Figure 11). We attribute this to the model inducing excessive fracture permeability that bleeds off overpressures prematurely. The majority of the disparity in the distribution consists of modeled pressures in excess of observed (lighter patches on Figure 11). The primary culprit for this difference is most likely an overestimate of TOC in the marginal lacustrine facies. However, an inaccurate geologic and thermal history may simply induce erroneous timing of maximum oil generation and associated overpressures.

Another disparity is that the model's overpressures only begin to decrease at the Duchesne fault zone (Figure 10), while observed overpressures terminate abruptly and completely at the fault zone (Figure 3). The fault zone probably represents a

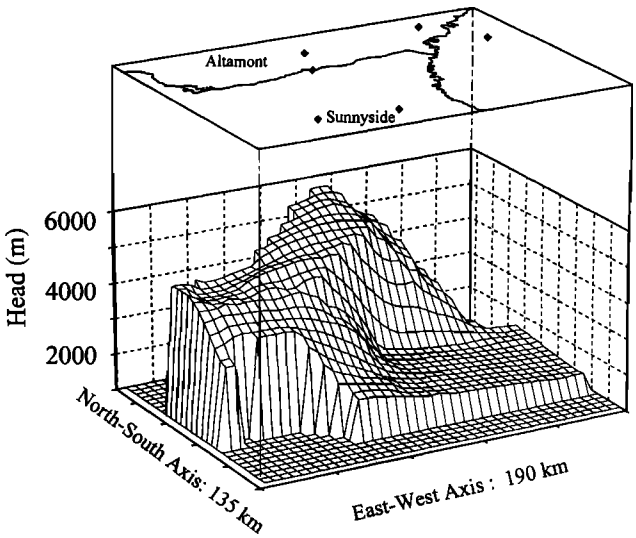

Figure 10. Isometric projection of modeled hydraulic head in the Flagstaff member of the Green River Formation within the Uinta basin (present day).

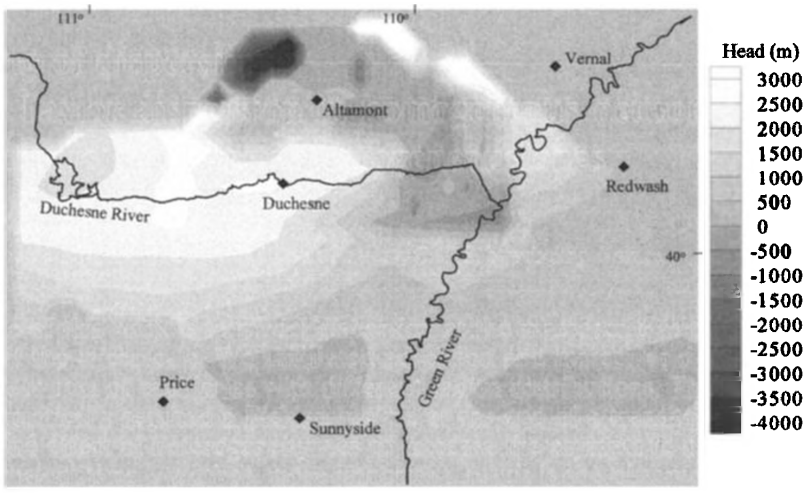

Figure 11. Map of disparity between modeled overpressure and observed overpressures, or h = modeled head − observed head, in the Flagstaff member of the Green River Formation.

region of high permeability; when we assigned this region a higher permeability distribution in the model, the resulting overpressure mapping was more consistent with that observed. The alternative end-member early uplift model results in a similar, qualitative match between model and observed overpressures. All of our results suggest that the basin's burial history and associated thermal history, regardless of "where" it lies between these end-member cases, will create and maintain overpressures in the Uinta basin. Both end-member structural histories, and we assume any realistic history in between, combined with reasonable model parameters of TOC, oil viscosity, etc., can qualitatively emulate the observed overpressure distribution. As mentioned previously, modeled overpressures are not directly sensitive to the burial history per se. The critical aspect is the timing and duration of peak temperatures in the thermal history (directly determined by the burial history) because this controls the peak and duration of oil generation and associated pressures (Figure 9). For the Uinta basin specifically, then, it is not the structural history alone that controls overpressuring. Associated temperature histories and the evolution of individual rock and multiphase fluid properties play the critical role.

In this context, we performed a sensitivity analysis to isolate threshold values of rock and fluid properties necessary for overpressure development. We tested permeability, relative permeability, porosity, capillary pressure, TOC, oil density, and oil viscosity. Surface temperature was another variable considered in the sensitivity tests, and associated results are described in the subsequent section of this paper. Basal heat flux was not tested in our sensitivity analysis inasmuch as we already understand its direct effect on overpressure generation; higher or lower basal heat flux simply changes the timing and magnitude of peak oil generation. Also, we are confident that basal heat flow is well constrained, compared to rock and fluid properties at depth, based on calibration described in detail by *McPherson* [1996].

Our sensitivity results revealed fluid pressures are most sensitive to permeability, TOC, and oil viscosity. Porosity and relative permeability are also significant, but the porosity effect manifests itself through associated permeability, and relative permeability is a scaling factor of absolute permeability. For each of the three parameters we ran a series of model simulations in which the individual parameter within a single finite difference cell was assigned a fixed value for the duration of the history simulation, whereas all other parameters in all other cells vary as described previously. In all simulations the late uplift model with the constant surface temperature condition was used, and the specific cell we evaluated corresponded to the Flagstaff member of the Green River Formation near the northern edge of the Altamont oil field. The depth of the selected cell is 4.2 km, with ambient properties of $\sim 2 \times 10^{-18}$ m^2 horizontal permeability, 1.6% TOC, and 0.5 cP viscosity.

Among the three parameters, permeability is the most important because it is a limiting factor that determines whether overpressures will occur due to any mechanism. The sensitivity study revealed an interval of permeability below which overpressures always form and above which overpressures do not form, as displayed in Figure 12a. Each point on the plot represents the maximum overpressure reached in a single finite difference cell in the Flagstaff member during a model simulation in which that cell and all cells connected to it were assigned the same, constant value of permeability. We tested the range of permeability from 10^{-19} m^2 to 5×10^{-18} m^2, as shown by the abscissa on Figure 12a. Results show that for values of permeability less than 10^{-18} m^2, overpressures are not sensitive to permeability. In other words, if permeability is lower than 10^{-18} m^2, overpressures always occur, at least for these specific conditions of temperature history, TOC, porosity, etc. We refer to this lower limit of sensitivity as the "always overpressure" value of permeability, or k_{aop}. Below the value of k_{aop} the maximum overpressure reached in the cell was ~51 MPa, the value of the least principal stress. In every simulation in which the fixed permeability was lower than k_{aop} and fluid pressure reached the least principal stress, the cell of interest fractured, and pressure decreased.

For the sequence of permeability values greater than 10^{-18} m^2, the maximum overpressure reached was less for each increase in fixed permeability (Figure 12a), and at 5×10^{-18} m^2, no appreciable overpressure developed. Overpressures only form for fixed permeability values less than 5×10^{-18} m^2. We

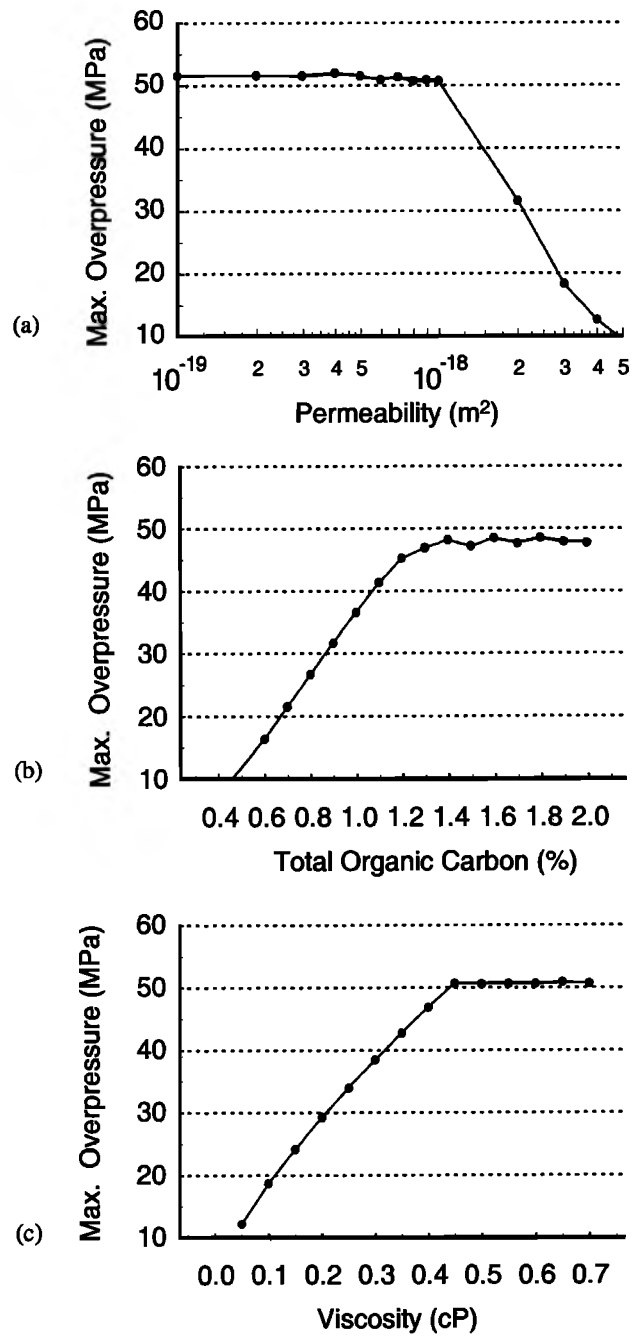

Figure 12. Results of overpressure sensitivity analysis: maximum overpressure versus (a) fixed permeability, (b) initial TOC content, and (c) fixed oil viscosity.

refer to this upper limit of sensitivity as the "threshold" value of permeability. Note also that for values of permeability greater than 10^{-18} m^2, the maximum overpressure reached was less than the least principal stress, and thus the cell of interest did not fracture. In all model simulations except the sensitivity analysis models, the minimum permeability assigned to any cell in the model was $\sim 10^{-18}$ m^2, as indicated by Figure 5.

In all basin history simulations except the sensitivity analyses, permeability of all strata evolved by the same formulation (Figure 5). An alternative, however, is to acknowledge lithological variations in permeability and assign alluvial strata a somewhat higher permeability (for example, an order of magnitude higher) than what is assigned to lacustrine strata. Results for models with this alternative parameterization resulted in slightly diminished overpressures in lacustrine facies and no overpressure development in alluvial facies, provided other variables favor overpressure development. We used a permeability anisotropy ratio of $K_v = K_h/1000$, as the permeability/porosity data suggest (Figure 5).

Similar results were obtained for the TOC sensitivity simulations. Figure 12b plots the maximum overpressure reached for fixed TOC ranging from 0.4 to 1.7%. The value of source rock TOC for which overpressuring always occurs, or TOC_{aop}, is about 1.2%, and the threshold value is about 0.5%; that is, for values of TOC greater than 1.2%, the maximum overpressure reached, met, or exceeded the least principal stress, and for values of TOC less than 0.5%, no appreciable overpressures developed.

The sensitivity study also suggested that if TOC is too high or initial permeability is too low, overpressures are created but not sustained for very long. If assigned TOC is much higher than 5%, or permeability assigned is much less than 10^{-18} m^2, then overpressures grow much more rapidly and peak at higher values. Fracture density is increased to the extent that overpressures dissipate rapidly and are not maintained as long because of the induced high fracture permeability.

The results of the oil viscosity sensitivity models are similar in character to those of TOC and permeability. A range of 0.0 cP up to 10 cP was tested, but the value at which overpressuring always occurs, or μ_{oap}, was just less than 0.5 cP, and the threshold value was about 0.05 cP (Figure 12c). The maximum viscosity for the deep Flagstaff dictated by the *Chew and Connally* [1959] correlation approaches 2 cP, well above the μ_{oap} of 0.45 cP (Figure 12c).

The typical values of permeability, TOC, and oil viscosity in the deep Flagstaff at Altamont, as determined by rock and oil samples, exceed the k_{oap}, μ_{oap}, and TOC_{oap} values determined by the sensitivity study. This explains why the model qualitatively reproduces observed overpressures, regardless of which end-member geologic history (and associated thermal history) is simulated.

6.5. Overpressure Maintenance: Fracture Permeability

Our modeling revealed that whether overpressures are maintained to present day depends on many factors, especially primary permeability and secondary fracture permeability. A surprising realization from the evolution simulations is that subsurface permeability is affected by surface temperature. Surface temperature affects temperature at depth and therefore the oil generation and overpressure history. Overpressures can induce rock fractures and increase permeability. The model simulations clearly show feedback between surface temperature and fracture permeability. In most simulations we held the surface temperature constant at 11°C, the current average surface temperature of the region today [*National Oceanic and Atmospheric Administration* (*NOAA*), 1989] throughout the basin's history to isolate the effects of the evolving structure on subsurface temperature. In some simulations, surface temperature was varied through time. The specific history applied (Figure 13) was modified from a surface temperature history of the Pacific Northwest [*Wolfe*, 1978] as described by *McPherson* [1996]. Subsurface temperature histories for the early uplift model of strata at the northern edge of the Altamont field (triangle on Figure 1) are displayed in

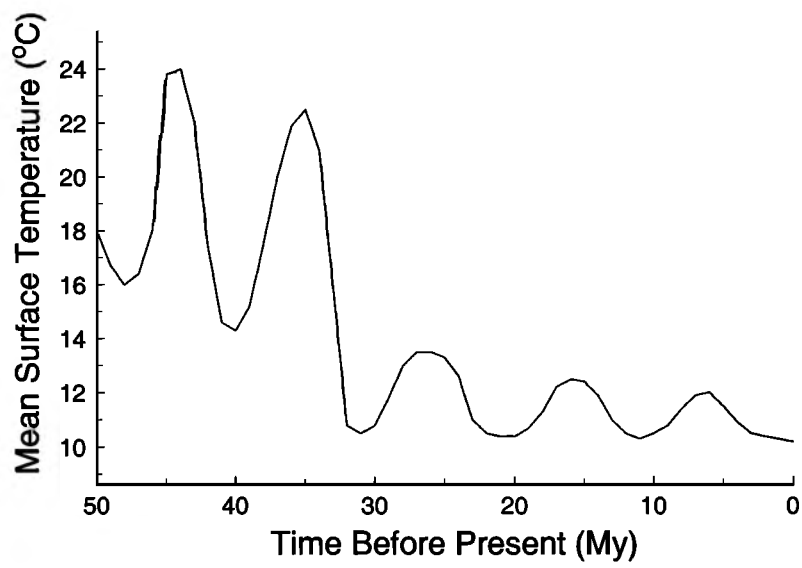

Figure 13. Surface temperature history assigned to Uinta basin. Adapted from *Wolfe* [1978].

Figure 14. Results of two simulations were compared, including one with a constant surface temperature boundary condition (Figure 14a) and one with a variable surface temperature history boundary condition (Figure 14b). The greatest effects of the variable surface temperature history on subsurface temperatures occur after 35 Ma, where disparities as much as 8°C exist between the different subsurface temperature histories. The differences occur because a greater surface temperature propagates to depth. Subsurface temperatures for the variable surface temperature history are always greater than those for constant surface temperature models, simply because all temperatures in the variable history tend to be >11°C (the value of the constant surface temperature).

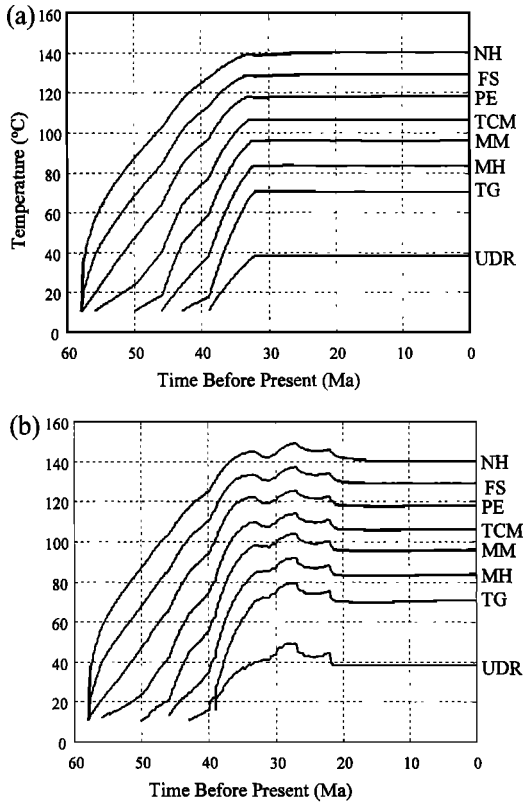

Figure 14. Temperature histories for strata in northern section of Altamont oil field. (a) Temperature history for early uplift model, constant surface temperature boundary condition. (b) Temperature history for early uplift model, variable surface temperature history boundary condition. See caption of Figure 7 for key of abbreviations.

The effect of subsurface temperature on fracture permeability and overpressure maintenance is demonstrated by results of the early uplift model with a constant surface temperature boundary condition; this model overpredicts pressures by 15 MPa in the deepest part of the Flagstaff. The fluid pressure histories produced by the early uplift model with constant surface temperature conditions for strata at the northernmost edge of the Altamont field (Figure 15a) can be compared to the maximum observed overpressure, 27.5 MPa, shown in the observed fluid pressure profile (Figure 4). However, the same model using the variable surface temperature history (Figure 14b) underpredicts the final values of overpressure by about 12.5 MPa (Figure 15b). Subsurface temperatures in the variable surface temperature model are always higher, producing greater peaks of oil generation and creating more fracture permeability. Final fluid pressures in the higher permeability environment drop at a faster rate and to a lower value (Figure 15).

Closer examination of both sets of fluid pressure histories (Figure 15) suggests that a trade-off between induced fracturing and oil generation must occur for the final value of overpressure to be consistent with the observed value. For example, the early uplift model with variable surface temperature history underpredicts the final value of overpressure (Figure 15b). However, this occurs because initial overpressures are higher in this model (Figure 15a) and, consequently, many more fractures are induced, creating higher permeability than in the same model with constant surface temperature. In both cases, four of the nine model layers are significantly overpressured during much of the modeled basin history, but higher overpressures are maintained longer in those formations that are less fractured because the permeability in those formations is

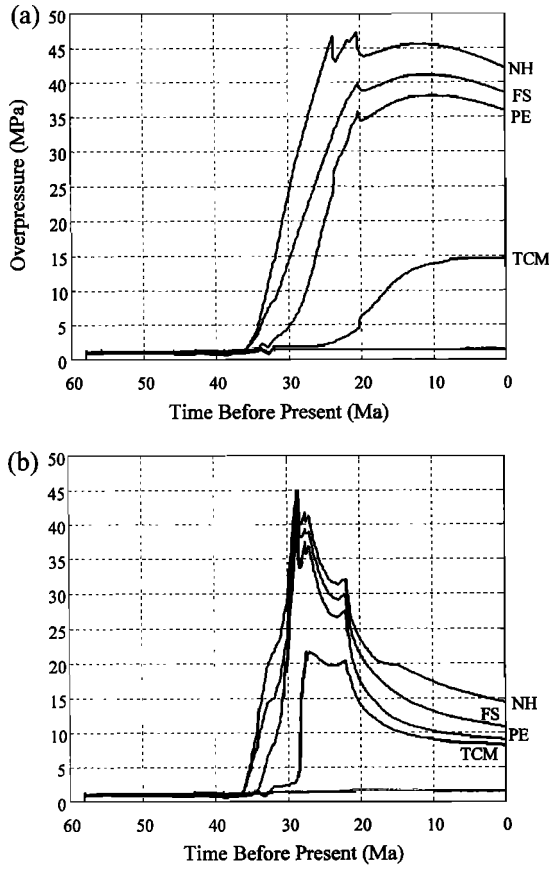

Figure 15. Overpressure histories for strata in northernmost Altamont field, early uplift model, with different surface temperature boundary conditions: (a) overpressure histories for early uplift model with constant surface temperature boundary condition; (b) overpressure histories for early uplift model with variable surface temperature history boundary. See caption of Figure 7 for key of abbreviations.

lower. Note that in both models the North Horn Formation is overpressured, even though it is not a source rock. The proximity of the North Horn to the highly pressured Flagstaff stratigraphically above, combined with its low permeability, causes the modeled overpressures in that formation. Of the three layers of Green River Formation that are overpressured, only the Flagstaff member is open lacustrine; the other two are marginal lacustrine and thus have a lower TOC content and oil generation potential.

6.6. Overpressures Caused by Pore Space Compaction

Other mechanisms of Green River Formation overpressures have been proposed, including pore compaction associated with sedimentary loading (J. J. Sweeney, written communication, 1993) and excessive dewatering of clays associated with transformation of smectite to illite within low-permeability strata. In this paper we demonstrate that ongoing oil generation sufficiently explains observed overpressures in the Tertiary Green River Formation. The model results suggest that pore compaction may have contributed to overpressures during periods of high sedimentation but that these overpressures dissipated relatively rapidly. Plotted on Figure 16 are portions of the fluid pressure histories corresponding to the late uplift model described previously. When the model was run with either oil generation or compaction inactive, significant overpressures were not induced (lower curve on Figure 16) during the period between 39 and 32 Ma. However, if both oil generation and compaction were active, some overpressuring was induced (top curve on Figure 16).

The most important conclusion from this particular sensitivity study is that the presence of oil was necessary for pore space compaction to cause overpressures. The oil generation rate during this particular period of the basin history was not high enough to produce overpressures, but the presence of oil reduced the relative permeability of water such that pore compaction became significant: ~12 MPa above normal fluid pressure (Figure 16), compared to oil-generated overpressures of almost 40 MPa in the same strata later in the history (Flagstaff, Figure 15a). Once deposition of the Duchesne River Formation ceases at 32 Ma, compaction ceases to be a significant overpressure mechanism. Simulation results suggest that overpressures due to pore space compaction could be significant and maintained for significant geologic time if absolute permeability were much lower, for example, less than 10^{-20} m^2, or if compressibility were increased (see Appendix A). However, a shift in compressibility shifts the modeled porosity trend to be inconsistent with the observed porosity trends.

7. Conclusions

The primary goal of this study was to provide a more detailed assessment of overpressures by oil generation in the Uinta basin, Utah, including the relative effects of the 3-D geologic history, thermal history, and multiphase fluid aspects. To achieve this goal, we developed a three-dimensional, numerical model of the evolution of the basin. The model was developed from a public domain computer code, with addition of a new mesh generator that builds the basin through time, coupling the structural, thermal, and hydrodynamic evolution, and including in situ hydrocarbon generation and multiphase migration. The multiphase flow aspects distinguish this model from previous models of the Uinta basin [*Bredehoeft et al.*, 1994]. Results suggest that explicit treatment of multiphase flow, including relative permeability, capillarity, variable den-

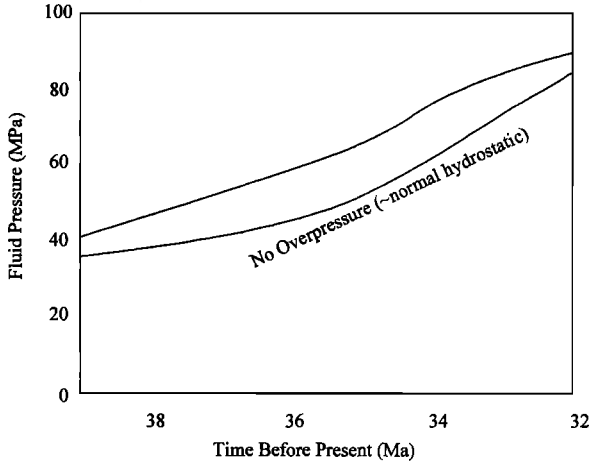

Figure 16. Selected window of the fluid pressure history for the Flagstaff member of the Green River Formation, illustrating that compaction contributes to modeled overpressures.

sity, and viscosity, is necessary to quantitatively estimate (by modeling) the possible magnitude and duration of overpressures by oil generation in a sedimentary basin.

We simulated evolution of the Uinta basin using two "end-member" extremes of its possible structural histories. Qualitative matching of modeled and observed overpressures affirms our hypothesized range of these conceptual history models, especially considering the complexity of the numerical model and its parameterization.

A general conclusion of this study is that knowledge of a basin's burial history is necessary to evaluate oil-generated overpressures. On the other hand, a priori measurements of overpressure may constrain the possible geologic history (even in 3-D), inasmuch as overpressure magnitudes restrict the possible thermal and associated petroleum generation histories. For the Uinta basin case study specifically, the entire range of assumed geologically realistic structural histories (both proposed end-member cases and all permutations in between) produce 3-D thermal histories that generate sufficient oil to qualitatively match observed overpressures in the basin. In other words, uncertainty in the structural history does not alter the conclusion that oil generation causes the observed overpressures. Additionally, depending on the specific parameterization used, both history models are consistent with regards to induced fractures in the northern Uinta basin, which is well known for its high fracture density.

Sensitivity study results elucidated the relative overpressuring roles of multiphase fluid interaction, oil properties, rock permeability, and depositional compaction. "Threshold" values of certain parameters for overpressures to develop were identified: oil viscosity 0.05 cP or higher, intrinsic permeability 5×10^{-18} m^2 or lower, and TOC values of 0.5% or higher. Most or all of these specific threshold values must be met or exceeded, depending on the structural history imposed, for overpressures to be develop. The sensitivity analysis also elucidated values of viscosity, TOC, and permeability, above or below which overpressures always develop. Results show that if oil viscosity is greater than 0.45 cP, permeability is less than 10^{-18} m^2, or TOC is greater than 1.2%, fluid pressures always rise to or exceed the least principal stress. Typical k, μ, and TOC of the deep Flagstaff at Altamont, as determined by rock and oil samples, approach or exceed these values determined by the sensitivity study, thus explaining why the model qualitatively reproduces observed overpressures.

Finally, the most important conclusions of this study are as follows:

1. Overpressures by oil generation create conditions for rock fracturing, and associated fracture permeability may regulate or control the propensity to maintain overpressures.

2. Higher surface temperatures (histories) cause shorter periods of very high oil generation rates, creating very high overpressures, associated fracturing, and higher fracture permeability. The model simulations clearly demonstrate feedback between surface temperature and fracture permeability.

3. A trade-off between induced fracturing and oil generation must occur for final modeled overpressures to be consistent with the observed values.

4. A necessary condition for pore compaction to cause detectable overpressures is the presence of significant amounts of oil, which reduces relative permeability. In the absence of oil, intrinsic permeability is not sufficiently low, and pore space compaction does not cause excess fluid pressures. This result is specific to, but probably not unique to, the Uinta basin.

Appendix A: Porosity Reduction by Sedimentary Compaction

The continuity equation for flow through a differential volume element, $\Delta x \Delta y \Delta z$, can be stated as

$$\nabla \cdot \rho v = \frac{\partial(\Delta M)}{\partial t} \Big/ (\Delta x \Delta y \Delta z), \tag{A1}$$

where ρ is the density of the fluid, v is the fluid flux, and M is the fluid mass within the volume element [*Jacob*, 1950; *Bredehoeft and Cooley*, 1983]. We assume that changes in the lateral dimensions are negligible but that the z dimension may change (e.g., due to depositional compaction). The rate of change of the fluid mass through time may then be stated as

$$\frac{\partial(\Delta M)}{\partial t} = \left[\phi(\Delta z)\left(\frac{\partial \rho}{\partial t}\right) + \rho(\Delta z)\left(\frac{\partial \phi}{\partial t}\right) + \rho\phi\left(\frac{\partial(\Delta z)}{\partial t}\right) \right] \Delta x \Delta y. \tag{A2}$$

Following *Jacob* [1950], if it is assumed that the change in volume of solids is negligible compared to the change in porosity, then

$$\frac{\partial(\Delta z)}{\partial t} = -\alpha \Delta z \left(\frac{\partial(\sigma_e)}{\partial t}\right), \tag{A3}$$

where α is vertical compressibility and σ_e is effective stress. The compressibility functions we used to parameterize the Uinta basin model are described by *McPherson and Garven* [1999]. Additionally, the change in porosity is

$$\frac{\partial \phi}{\partial t} = -\alpha(1 - \phi)\left(\frac{\partial \sigma_e}{\partial t}\right) \tag{A4}$$

and the change in density is

$$\frac{\partial \rho}{\partial t} = \beta \rho \left(\frac{\partial p}{\partial t}\right) \tag{A5}$$

where β is the compressibility of the fluid and p is the pore pressure. Combining (A2) through (A5) and introducing the effective stress law yields the following form of the flow equation:

$$-\nabla \cdot \rho v = \phi\rho\left(\beta + \frac{\alpha}{\phi}\right)\frac{\partial p}{\partial t} - \rho\alpha \frac{\partial \sigma_T}{\partial t}. \tag{A6}$$

This equation, minus the last term on the right-hand-side, is another form of the basic continuity equation solved by TOUGH2.

Finally, compaction, uplift, and subsidence require that the depth z of the volume element change through time. The condition of a changing z requires that (A6) becomes

$$-\nabla \cdot \rho v = \phi\rho\left(\beta + \frac{\alpha}{\phi}\right)\left(\frac{Dp}{Dt}\right) - \rho\alpha\left(\frac{D\sigma_T}{Dt}\right), \tag{A7}$$

where D indicates the total derivative (changes in the x and y dimensions are still considered negligible). This expression can be rewritten as

$$-\nabla \cdot \rho v = \phi\rho\left(\beta + \frac{\alpha}{\phi}\right)\left(\frac{\partial p}{\partial t} + \frac{\partial p}{\partial z}\frac{\partial z}{\partial t}\right) - \rho\alpha\left(\frac{\partial \sigma_T}{\partial t} + \frac{\partial \sigma_T}{\partial z}\frac{\partial z}{\partial t}\right), \quad \text{(A8)}$$

where $\partial z/\partial t$ is the rate of subsidence, uplift, erosion, and/or sedimentation. Separating the basic flow equation from (A8), the remaining source terms are

$$\phi\rho\left(\beta + \frac{\alpha}{\phi}\right)\left(\frac{\partial p}{\partial z}\frac{\partial z}{\partial t}\right) - \rho\alpha\left(\frac{\partial \sigma_T}{\partial t} + \frac{\partial \sigma_T}{\partial z}\frac{\partial z}{\partial t}\right). \quad \text{(A9)}$$

The terms in expression (A9) are the source/sink terms we added to the flow equation to account for changes in fluid mass balance due to compaction in a moving medium. *McPherson* [1996] provides a more detailed discussion of this derivation.

Acknowledgments. The authors wish to acknowledge the U.S. Department of Energy for a grant that supported this work (DOE DE-AI03-93-ER14338/A000). Additional funding and many other types of support were provided by the U.S. Geological Survey. This work is part of the Ph.D. dissertation research of the senior author, Brian McPherson. John Bredehoeft (formerly of the U.S. Geological Survey) and Dave Chapman (University of Utah) were both Ph.D. advisors of Brian McPherson, and both provided absolutely stellar advice, encouragement, and the best of both worlds in terms of geophysical and hydrogeological training.

References

Allen, P. A., and J. R. Allen, *Basin Analysis: Principles and Applications*, Blackwell Sci., Malden, Mass., 1992.

Anders, D. E., J. G. Palacas, and R. C. Johnson, Thermal maturity of rocks and hydrocarbon deposits, Uinta Basin, Utah, in *Hydrocarbon and Mineral Resources of the Uinta Basin, Utah and Colorado, Utah Geol. Assoc. Guideb.*, vol 20, edited by T. D. Fouch, V. F. Nuccio, and T. C. Chidsey Jr., pp. 53–76, Utah Geol. Assoc., Salt Lake City, 1992.

Bethke, C. M., Inverse hydrologic analysis of the distribution and origin of gulf coast-type geopressured zones, *J. Geophys. Res.*, *91*, 6535–6545, 1986.

Bredehoeft, J. D., and R. L. Cooley, Comment on "A note on the meaning of storage coefficient" by T. N. Narasimhan and B. Y. Kanehiro, *Water Resour. Res.*, *19*, 1632–1634, 1983.

Bredehoeft, J. D., R. G. Wolff, W. S. Keys, and E. Shuter, Hydraulic fracturing to determine the regional in situ stress field, Piceance Basin, Colorado, *Geol. Soc. Am. Bull.*, *87*, 250–258, 1976.

Bredehoeft, J. D., J. B. Wesley, and T. D. Fouch, Simulations of the origin of fluid pressure, fracture generation, and the movement of fluids in the Uinta basin, Utah, *AAPG Bull.*, *78*, 1729–1747, 1994.

Chapman, D. S., and K. P. Furlong, Thermal state of the continental lower crust, in *Continental Lower Crust, Dev. Geotectonics*, vol 23, edited by D. M. Fountain, R. Arculus, and R. M. Kay, pp. 179–199, Elsevier Sci., New York, 1992.

Chapman, D. S., T. H. Keho, M. S. Bauer, and M. D. Picard, Heat flow in the Uinta Basin determined from bottom hole temperature (BHT) data, *Geophysics*, *49*, 453–466, 1984.

Chew, J., and C. A. Connally, A viscosity correlation for gas-saturated crude oils, *Trans. Am. Inst. Min. Metall. Pet. Eng.*, *216*, 23–25, 1959.

Chidsey, T. C., and M. D. Laine, The fractured Green River and Wasatch formations of the Uinta Basin, Utah; targets for horizontal drilling, in *Hydrocarbon and Mineral Resources of the Uinta Basin, Utah and Colorado, Utah Geol. Assoc. Guideb.*, vol. 20, edited by T. D. Fouch, V. F. Nuccio, and T. C. Chidsey Jr., pp. 123–134, Utah Geol. Assoc., Salt Lake City, 1992.

Deming, D., Regional permeability estimates from investigations of coupled heat and groundwater flow, North Slope of Alaska, *J. Geophys. Res.*, *98*, 16,271–16,286, 1993.

Domenico, P. A., and F. W. Schwartz, *Physical and Chemical Hydrogeology*, John Wiley, New York, 1990.

Fouch, T. D., C. J. Wandrey, J. K. Pitman, V. F. Nuccio, J. W. Schmoker, D. D. Rice, R. C. Johnson, and G. L. Dolton, Natural gas accumulations in low permeability Tertiary and Cretaceous (Campanian and Maastrichtian) rock, Uinta basin, Utah, U.S., *Rep. DOE/MC/20422-3051 (DEC92001132)*, 81 pp., Off. of Fossil Energy, Dep. of Energy, 1992.

Franczyk, K. J., J. K. Pitman, and D. J. Nichols, Sedimentology, mineralogy, palynology, and depositional history of some uppermost Cretaceous and lowermost Tertiary rocks along the Utah Book and Roan Cliffs east of the Green River, *U.S. Geol. Surv. Bull.*, *1787-N*, 27 pp., 1990.

Garven, G., Continental-scale groundwater flow and geologic processes, *Annu. Rev. Earth Planet. Sci.*, *23*, 89–117, 1995.

Hintze, L. F., Geologic map of Utah, 2 sheets, *Utah Geol. Miner. Surv.*, *1:500,000*, 1980.

Hubbert, M. K., and W. W. Rubey, Role of fluids in mechanics of overthrust faulting, *Geol. Soc. Am. Bull.*, *70*, 115–205, 1959.

Jacob, C. E., Flow of ground water, in *Engineering Hydraulics*, edited by H. Rouse, pp. 321–386, John Wiley, New York, 1950.

Johnson, R. C., and V. F. Nuccio, Surface vitrinite reflectance study of the Uinta and Piceance basins and adjacent areas, eastern Utah and western Colorado—Implications for the development of Laramide basins and uplifts, *U.S. Geol. Surv. Bull.*, *1787-DD*, 1993.

Lucas, P. T., and J. M. Drexler, Altamont-Bluebell: A major fractured and overpressured stratigraphic trap, Uinta Basin, Utah, in *Deep Drilling Frontiers in the Central Rocky Mountains, Rocky Mountain Association of Geologists Symposium*, edited by D. W. Bolyard, pp. 265–273, Am. Assoc. of Pet. Geol., Tulsa, Okla., 1976.

McPherson, B. J. O. L., A three-dimensional model of the geologic and hydrodynamic history of the Uinta basin, Utah: Analysis of overpressures and oil migration, Ph.D. dissertation, 119 pp., Univ. of Utah, Salt Lake City, 1996.

McPherson, B. J. O. L., and G. Garven, Hydrodynamics and overpressure mechanisms in the Sacramento Basin, California, *Am. J. Sci.*, *299*, 429–466, 1999.

McPherson, B. J. O. L., R. D. Jarrard, and J. D. Bredehoeft, Controls on intergranular porosity and permeability in the northern Uinta basin, Utah, *U.S. Geol. Surv. Water Resour. Invest. Rep.*, in press, 2001.

Moridis, G. J., A new set of direct and iterative solvers for the TOUGH2 family of codes, *Rep. LBL-37200*, Lawrence Berkeley Lab., Berkeley, Calif., 1995.

Moridis, G. J., and K. Pruess, TOUGH simulations of Updegraff's set of fluid and heat flow problems, *Rep. LBL-32611*, Lawrence Berkeley Lab., Berkeley, Calif., 1992.

Narasimhan, T. N., and P. A. Witherspoon, An integrated finite difference method for analyzing fluid flow in porous media, *Water Resour. Res.*, *12*, 57–64, 1976.

Narr, W., and J. B. Currie, Origin of fracture porosity—Example from Altamont field, Utah, *AAPG. Bull.*, *66*, 1231–1247, 1982.

National Oceanic and Atmospheric Administration (NOAA), Utah climatological data, vol. 98, no. 1, Washington, D. C., 1989.

Neuzil, C. E., Groundwater flow in low-permeability environments, *Water Resour. Res.*, *22*, 1163–1195, 1986.

Neuzil, C. E., Abnormal pressures as hydrodynamic phenomena, *Am. J. Sci.*, *295*, 742–786, 1995.

Oldenburg, C. M., and K. Pruess, Numerical simulation of coupled flow and transport with TOUGH2: A verification study, *Rep. LBL-35273*, Lawrence Berkeley Lab., Berkeley, Calif., 1994.

Pitman, J. K., T. D. Fouch, and M. B. Goldhaber, Depositional setting and diagenetic evolution of some Tertiary unconventional reservoir rocks, Uinta basin, Utah, *AAPG Bull.*, *66*, 1581–1596, 1982.

Pruess, K., TOUGH user's guide, *Rep. LBL-20700*, Lawrence Berkeley Lab., Berkeley, Calif., 1987.

Pruess, K., TOUGH2—A general-purpose numerical simulator for multiphase fluid and heat flow, *Rep. LBL-29400*, Lawrence Berkeley Lab., Berkeley, Calif., 1991.

Pruess, K., and J. S. Y. Wang, TOUGH—A numerical model for nonisothermal unsaturated flow to study waste canister heating effects, in *Materials Research Society Symposia Proceedings*, vol. 26, pp. 1031–1038, North-Holland, New York, 1984.

Ryder, R. T., T. D. Fouch, and J. H. Elison, Early Tertiary sedimentation in the western Uinta Basin, Utah, *Geol. Soc. Am. Bull.*, *87*, 496–512, 1976.

Spencer, C. W., Hydrocarbon generation as a mechanism for overpressuring in Rocky Mountain Region, *AAPG Bull.*, *71*, 368–388, 1987.

Sweeney, J. J., A. K. Burhnam, and R. L. Bruan, A model of hydro-

carbon generation from type I kerogen: Application to Uinta basin, *AAPG Bull.*, *71*, 967–985, 1987.

Timko, D. J., and W. H. Fertl, Relationship between hydrocarbon accumulation and geopressure and its economic significance, *JPT J. Pet. Technol.*, *23*, 923–933, 1971.

Willett, S. D., and D. S. Chapman, On the use of thermal data to resolve and delineate hydrologic flow systems in sedimentary basins: An example from the Uinta Basin, Utah, in Proceedings of the Third Annual Canadian/American Conference on Hydrogeology; *Hydrology of Sedimentary Basins—Applications to Exploration and Exploitation*, edited by B. Hitchon, S. Bachu, and C. Sauveplane, pp. 159–168, Natl. Water Well Assoc., Dublin, Ohio, 1987.

Wolfe, J. A., A paleobotanical interpretation of Tertiary climates in the northern hemisphere, *Am. Sci.*, *66*, 694–703, 1978.

J. D. Bredehoeft, The Hydrodynamics Group, 16711 76th Ave. West, Edmonds, WA 98026.

B. J. O. L. McPherson, Hydrology Program, New Mexico Institute of Mining and Technology, Socorro, NM 87801. (brian@nmt.edu)

(Received September 28, 1999; revised August 3, 2000; accepted August 28, 2000.)